

# Effect of Northward Ageostrophic Winds Associated with a Tropical Cyclone on PRE Rainfall Enhancement

Kazuo Saito<sup>1,2,3</sup>, Takumi Matsunobu<sup>4</sup>, Tsutao Oizumi<sup>2</sup>

<sup>1</sup>Atmosphere and Ocean Research Institute/University of Tokyo, <sup>2</sup>Meteorological Research Institute, <sup>3</sup>Japan Meteorological Business Support Center, <sup>4</sup>Ludwig-Maximilians-University

## 1. Background

In Japan, heavy rainfalls often occur when a typhoon exists off the south coast of Japan (Fig. 1). This phenomenon is often explained by northward moisture transport by a typhoon, however, 'northward' emission from typhoon violates the relationship of geostrophic wind:

$$u_g = -\frac{1}{f} \frac{\partial \phi}{\partial y}, v_g = \frac{1}{f} \frac{\partial \phi}{\partial x}.$$

These pre-typhoon rainfalls are also known in other countries and called as 'PRE' (Fig. 2). PRE is enhanced by deep poleward moisture transport ahead of the recurving TC (Schumacher et al. 2011).

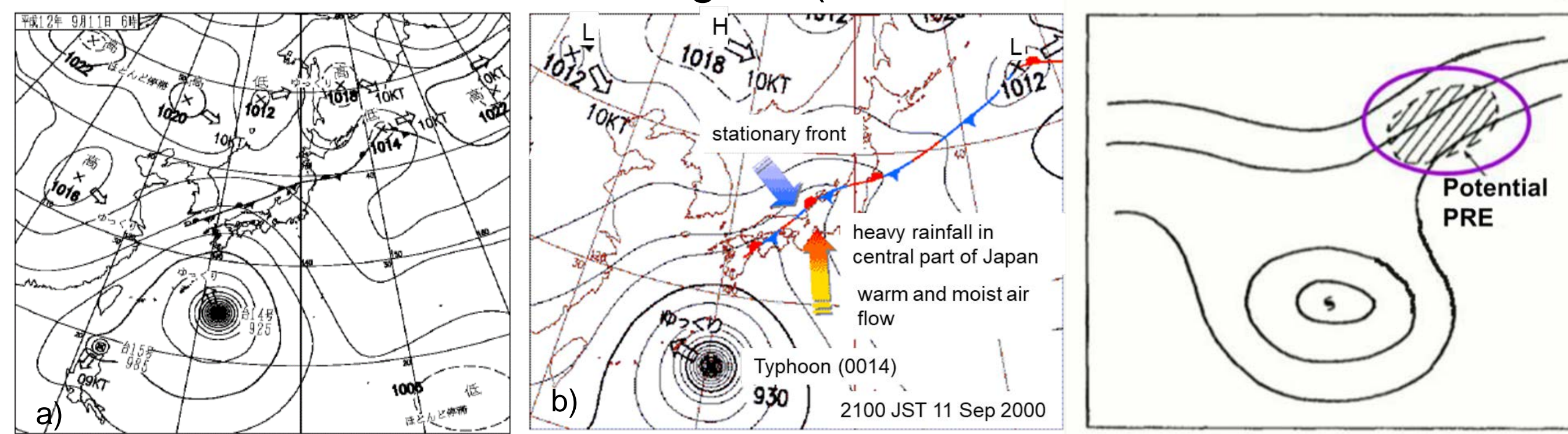


Fig. 1: a) Surface weather map at 2100 UTC Sep 10, 2000. b) Schematic explanation of the remote effect of the typhoon. After JMA homepage.

Fig. 2. Antecedent rainfall associated with TC. (Basart and Carr 1978; Cote 2007).

## 2. Ageostrophic winds with Typhoon Melor (T0918)

Typhoon Melor (0918) made landfall in central Japan on 8 October 2009. Considerable rainfall was observed over southern part of Japan along a stationary front at the pre-typhoon period. When the typhoon approached Japan, distinct ageostrophic southerly winds were observed over western part of Japan (Fig. 3).

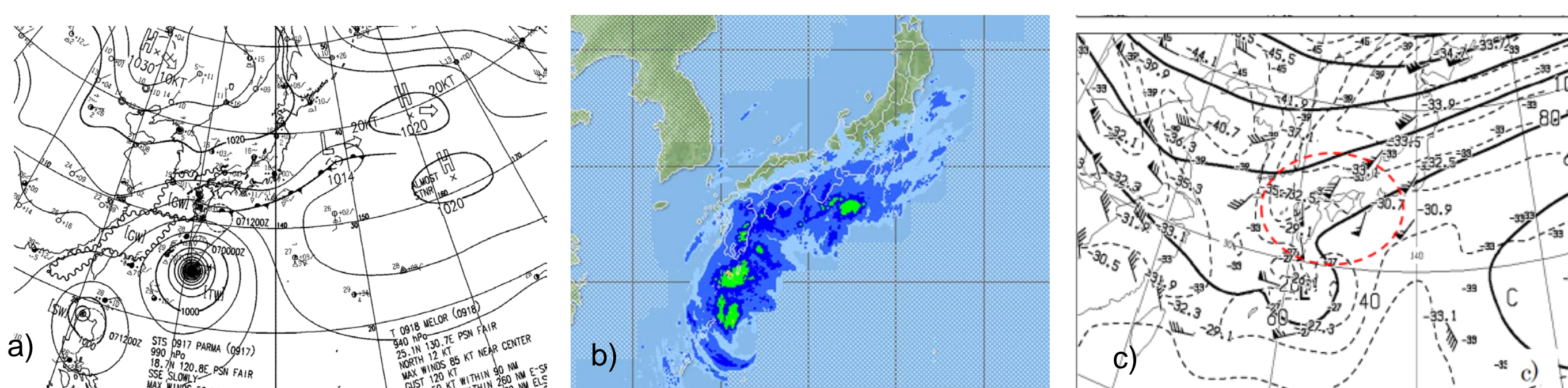


Fig. 3. a) Surface weather map at 1200 UTC 6 October 2009. b) Precipitation analysis of JMA at 00 UTC 7th October 2009. c) Subjective analysis by JMA at 300 hPa level and observed winds at 00 UTC 7 October 2009.

## 3. Simulated northerly winds and their origin

The northerly ageostrophic winds were well simulated by JMA nonhydrostatic model with a horizontal resolution of 10 km (Fig. 4).

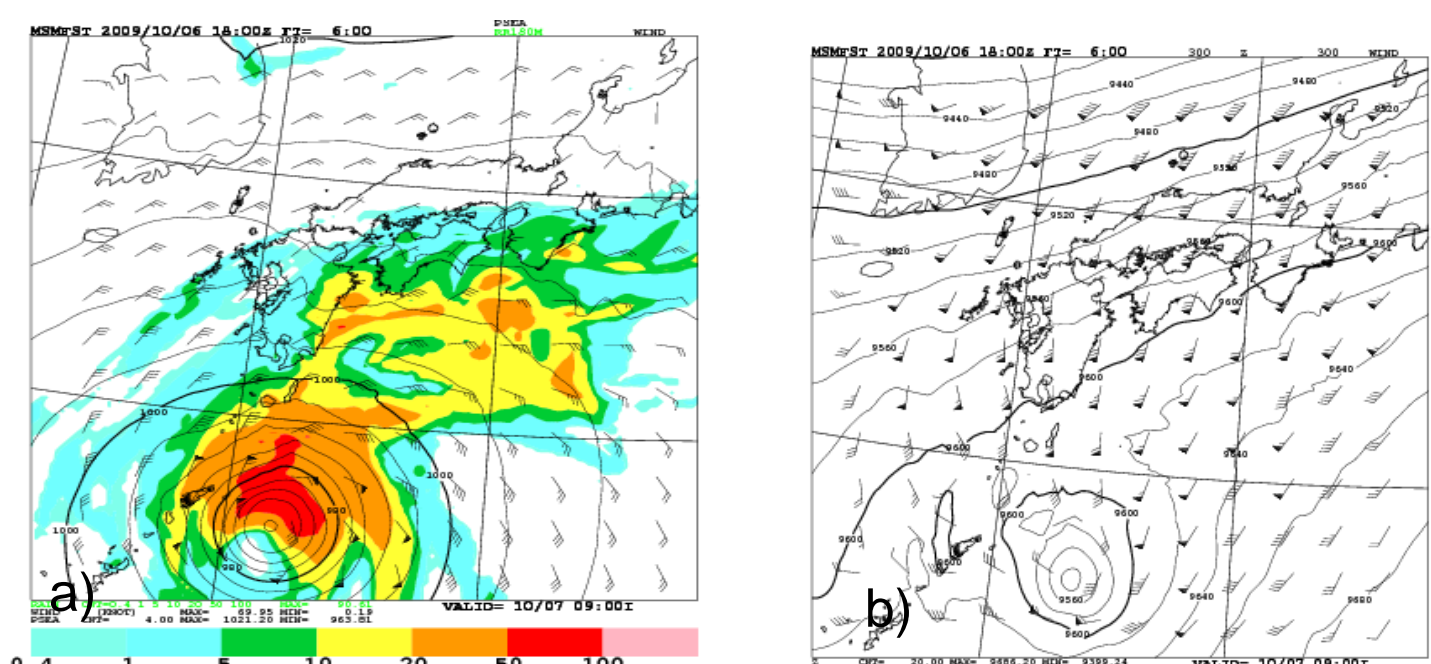


Fig. 4. a) Surface winds and mean sea level pressure with color shade of 3-hour accumulated precipitation predicted by JMA-NHM for 00 UTC 7 October 2009 (FT=6). b) Height field and horizontal winds at 300 hPa for 00 UTC 7 October.

These ageostrophic winds are explained by a relationship between the horizontal velocity acceleration and the ageostrophic motion (Haltiner and Martin 1957).

$$\frac{du}{dt} = fv - \frac{\partial \phi}{\partial x} = f(v_a + v_g) - \frac{\partial \phi}{\partial x} = fv_a, \quad (2)$$

$$\frac{dv}{dt} = -fu - \frac{\partial \phi}{\partial y} = -f(u_a + u_g) - \frac{\partial \phi}{\partial y} = -fu_a. \quad (3)$$

## 4. Northward moisture fluxes by ageostrophic winds

To evaluate the influence of the ageostrophic wind on PRE, we checked northward moisture fluxes by horizontal winds and the ageostrophic winds contribution. Figures 5a and 5b show northward moisture fluxes around  $z=9$  km (27<sup>th</sup> to 30<sup>th</sup> model levels) by horizontal and ageostrophic winds. Ageostrophic winds apparently enhance the moisture fluxes over the western Japan. Although the northward ageostrophic winds are remarkable in the upper levels (Fig. 5c), ageostrophic wind components contribute to enhance the deep poleward water vapor transport in middle and upper layers above 3 km (Fig. 5d).

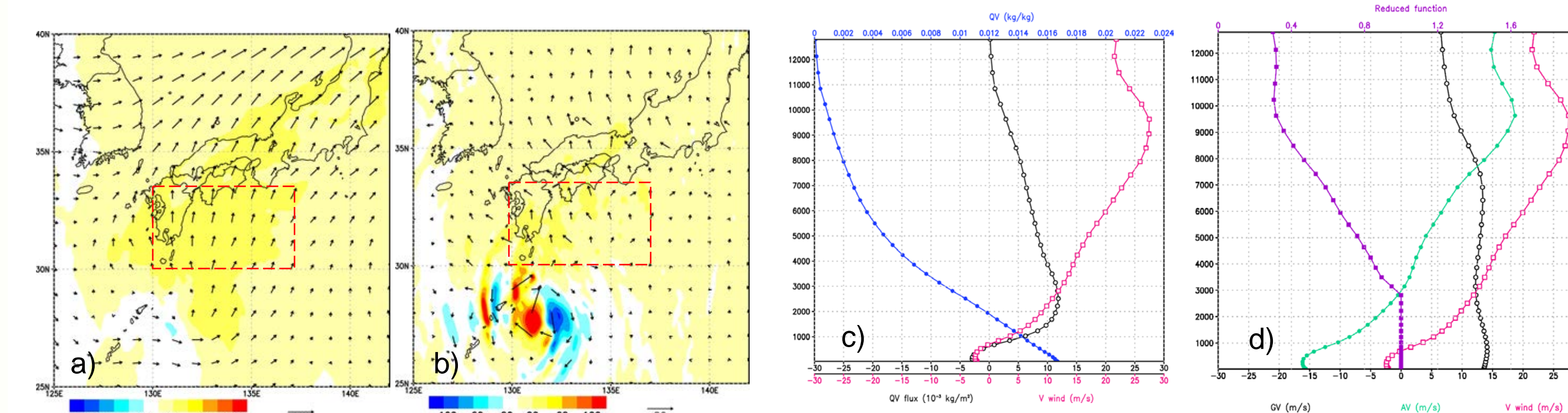


Fig. 5. a) Horizontal distribution of northward moisture fluxes by horizontal winds and b) ageostrophic winds. c) Vertical profiles of meridional geostrophic wind (red), northward moisture fluxes (black) and water vapor over a red broken rectangle area (130-137 E, 30-33 N). d) Vertical profiles of  $v$  (red),  $v_g$  (black),  $v_a$  (green) and the ratio of  $v_g$  to  $v$  ( $v_g/v$ ; purple, depicted by 1.0 for below 3 km).

## 5. Sensitivity experiment on moisture by ageostrophic winds

We reduced the model moisture at FT=6 (00UTC 7 Oct 2009) in middle and upper levels over the area off the south coast of Japan (130-137 E, 30-33 N) according to the contribution of the ageostrophic wind in the northward wind (Fig. 6), and restart the model. Precipitation over western Japan was decreased about 30% when the contributions in moisture fluxes by ageostrophic winds were removed (Fig. 7).

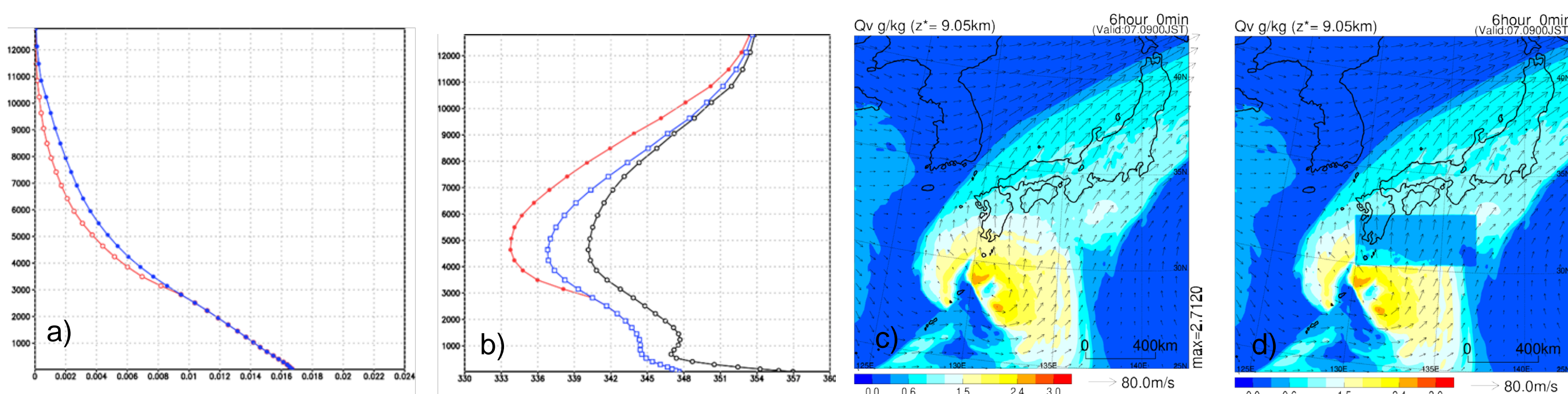


Fig. 6. a) Vertical profiles water vapor mixing ratio in CNTL (blue) and TEST (red) over a rectangle area around western Japan (130°E-137°E, 30°N-33°N). b) Same as in a) but equitable potential temperatures. Saturation equitable potential temperature is indicated by a black line. c) Horizontal winds (arrows) and water vapor mixing ratio by CNTL at  $z = 9$  km. d) Same as in c) except for TEST.

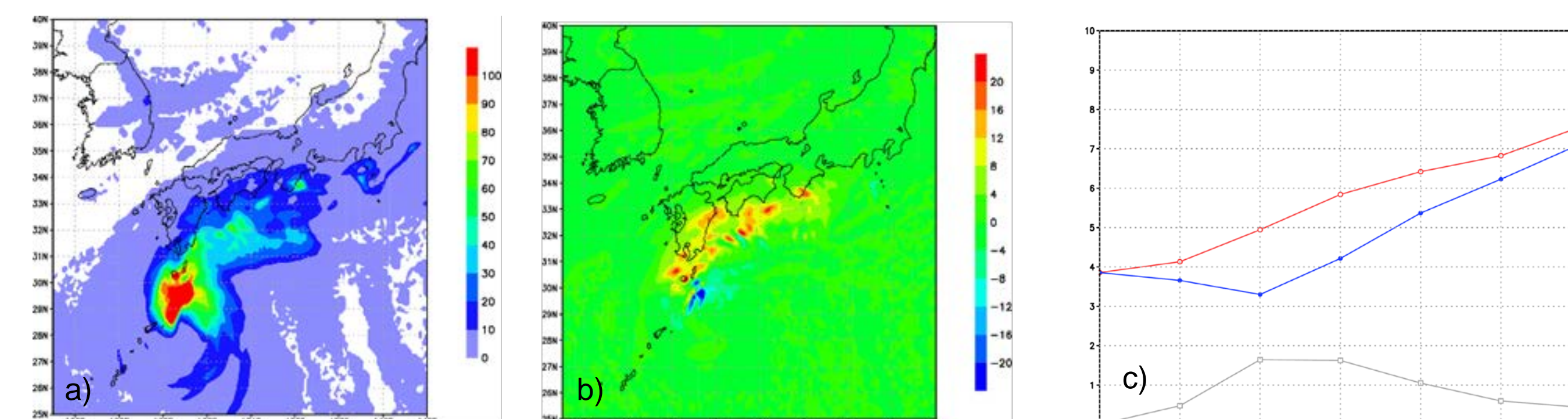


Fig. 7. a) Four-hour accumulated rain by CNTL at 04 UTC 7 October (FT=6-10). b) Decrease of accumulated precipitation (CNTL-TEST). c) Hourly precipitation intensities of CTL (red) and TEST (blue) averaged over western Japan (red rectangle; 130-137°E, 31-34°N).

## 6. Cloud resolving model experiment

We conducted a cloud resolving simulation using JMA-NHM with a horizontal resolution of 2 km. In the sensitivity experiment where the moisture in the middle and upper layers was reduced over the area off the south coast of western Japan, the water vapor reduction area was advected northward, and the snow in the middle and upper layers and the cloud ice in the upper layer decreased, reducing the rain below the melting level (Figs. 8 and 9). The maximum intensity of convective updrafts decreased by about 10% in the test experiment (Fig. 10).

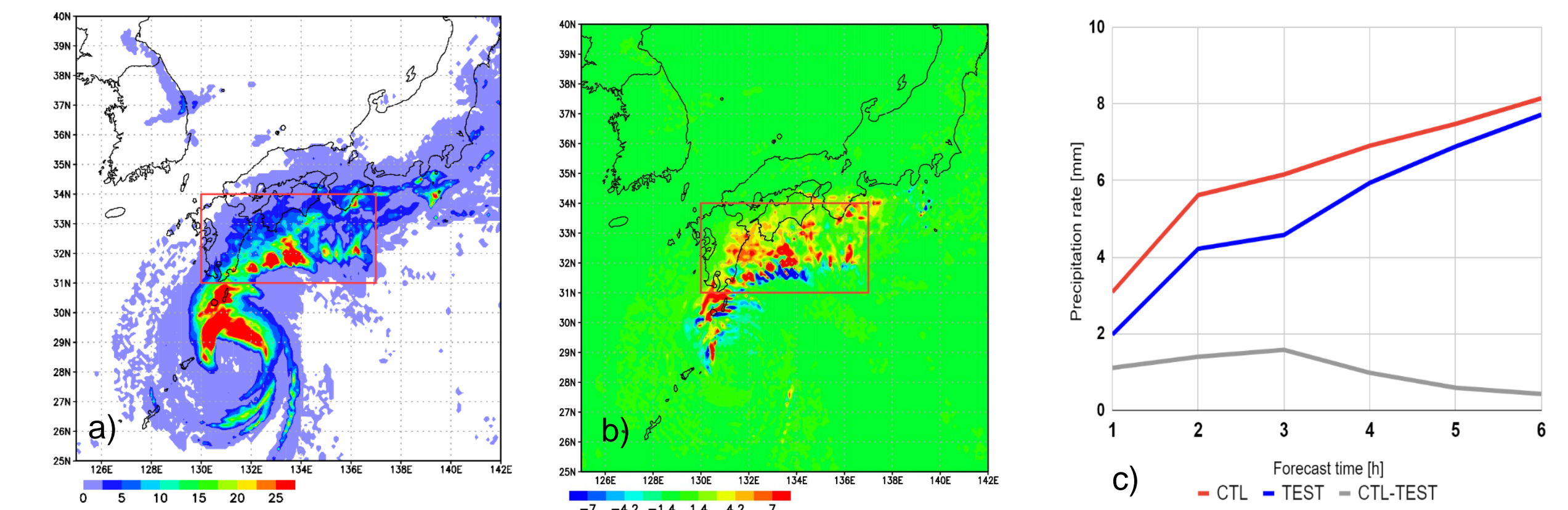


Fig. 8. a) One-hour precipitation intensity by CNTL of 2 km NHM at 03 UTC 7 October (FT=2-3). b) Same as in a) but by TEST. c) Difference (CNTL minus TEST). d) Hourly precipitation intensities of CNTL (red) and TEST (blue), and the difference (gray) averaged over western Japan (red rectangle; 130-137° E, 31-34° N).

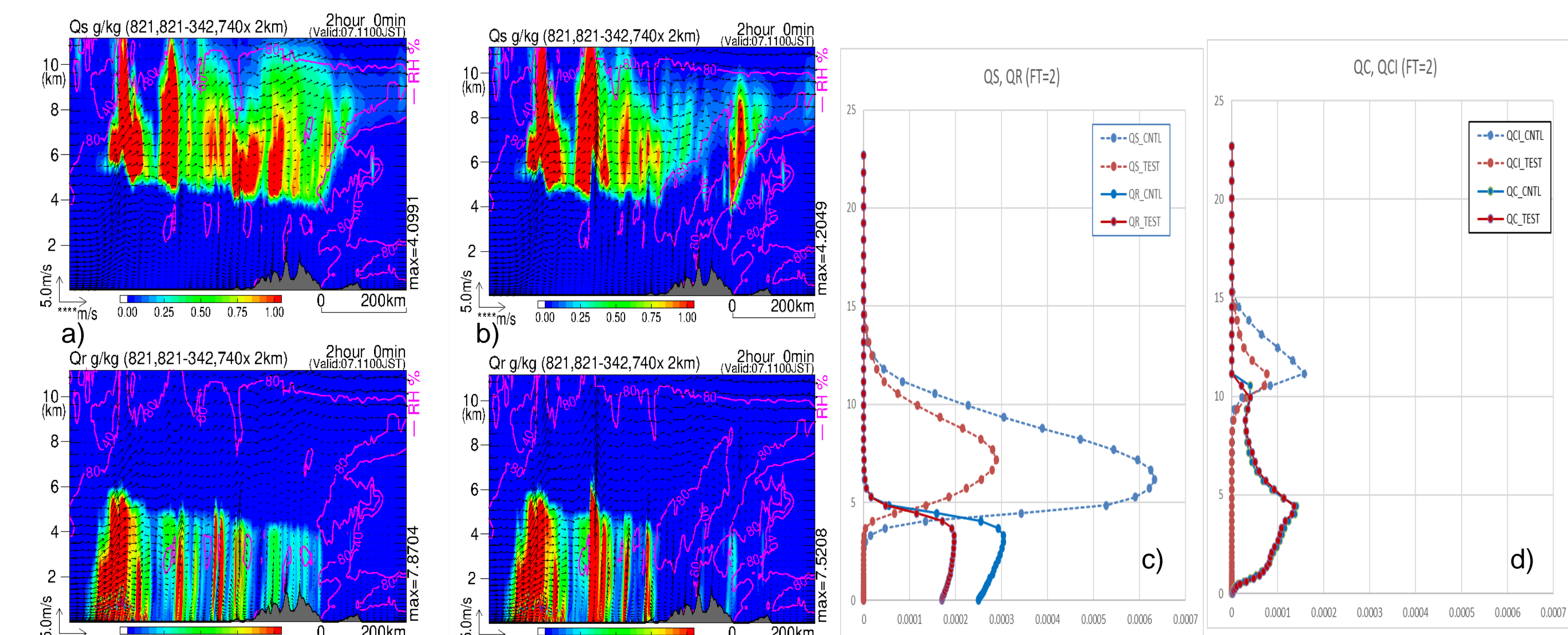


Fig. 9. a) Vertical cross-section of snow ( $Q_s$ ) and rain ( $Q_r$ ) along 132.5 E at 02 UTC 7 October (FT=2) by CNTL. Contours of relative humidity are depicted by purple lines. b) Same as in a) except for TEST. c) Vertical profiles of cloud microphysical quantities averaged over western Japan (red rectangle in Fig. 8; 130-137° E, 31-34° N) for snow (QS) and rain (QR) at 02 UTC 7 October (FT=2) in CNTL (blue) and TEST (brown). d) Same as in c) but for cloud ice (QCI) and cloud water (QC).

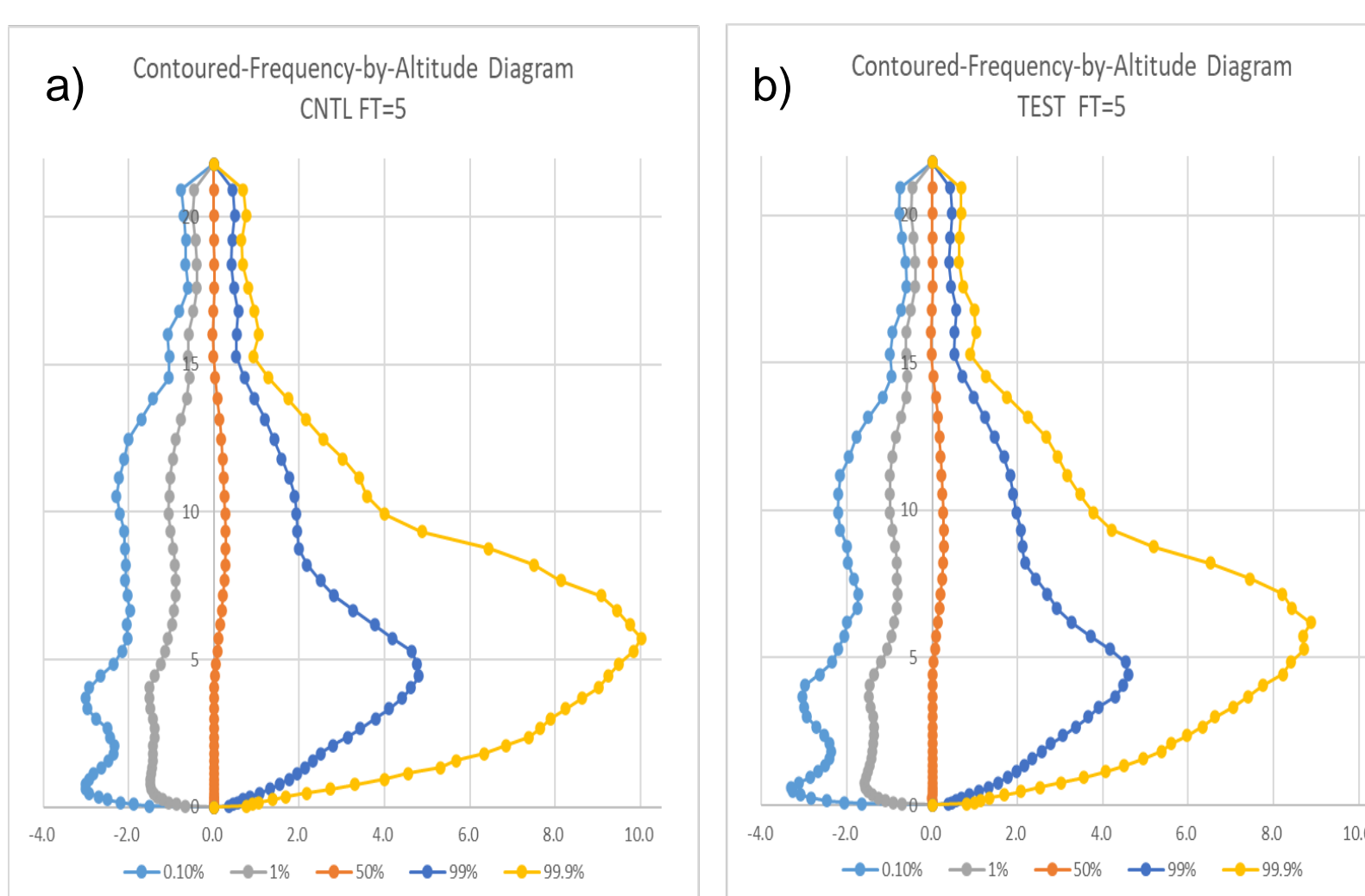


Fig. 10. a) Contoured Frequency by Altitude Diagram (CFAD) of vertical motion at FT=5 for CNTL over western Japan (130-137°E, 31-34°N). b) Same as in c) but for TEST.

References:  
Saito, K., 2019: On the northward ageostrophic winds associated with a tropical cyclone. *SOLA*, 15, 222-227. Saito, K., and T. Matsunobu, 2020: Northward ageostrophic winds associated with a tropical cyclone. Part 2: Moisture transport and its impact on PRE. *SOLA*, 16, 198-205.  
Saito, K., T. Matsunobu, and T. Oizumi, 2022: Effect of upper-air moistening by northward ageostrophic winds associated with a tropical cyclone on the PRE enhancement. *SOLA*, 18, 81-87.